

Optimality in self-organized molecular sorting

Marco Zamparo,^{1,2} Donatella Valdembri,^{3,4} Guido Serini,^{3,4} Igor V. Kolokolov,^{5,6,*}
Vladimir V. Lebedev,^{5,6,†} Luca Dall'Asta,^{2,1,7,‡} and Andrea Gamba^{1,2,8,§}

¹*Institute of Condensed Matter Physics and Complex Systems,
Department of Applied Science and Technology, Politecnico di Torino,
Corso Duca degli Abruzzi 24, 10129 Torino, Italy*

²*Italian Institute for Genomic Medicine (IIGM), Via Nizza 52, 10126 Torino, Italy*

³*Department of Oncology, University of Torino School of Medicine, Candiolo, 10060 Torino, Italy*

⁴*Candiolo Cancer Institute, Fondazione del Piemonte per l'Oncologia (FPO),
Istituto di Ricovero e Cura a Carattere Scientifico (IRCCS), Candiolo, 10060 Torino, Italy*

⁵*L.D. Landau Institute for Theoretical Physics, 142432,
Moscow Region, Chernogolovka, Ak. Semenova, 1-A, Russia*

⁶*National Research University Higher School of Economics, 101000, Myasnitskaya 20, Moscow, Russia*

⁷*Collegio Carlo Alberto, Via Real Collegio 30, 10024 Moncalieri, Italy*

⁸*Istituto Nazionale di Fisica Nucleare (INFN), Via Pietro Giuria 1, 10125 Torino, Italy*

We introduce a simple physical picture to explain the process of molecule sorting, whereby specific proteins and lipids are concentrated and distilled into nanometric lipid vesicles in eukaryotic cells. To this purpose, we formulate a model based on the coupling of spontaneous molecular aggregation with vesicle nucleation. Its implications are studied by means of a phenomenological theory describing the diffusion of molecules towards multiple sorting centers that grow due to molecule absorption and are extracted when they reach a sufficiently large size. The predictions of the theory are compared with experimental observations and with numerical simulations of a lattice-gas realization of the model. The efficiency of the distillation process is found to be optimal for intermediate aggregation rates, where the density of sorted molecules is minimal and the process obeys simple scaling laws. Quantitative measures of endocytic sorting performed in primary endothelial cells are compatible with the hypothesis that these optimal conditions are realized in living cells.

I. INTRODUCTION

To counter the homogenizing effect of diffusion, eukaryotic cells developed an elaborate system to sort and distill specific proteins into nanometric lipid vesicles, that are then transported towards appropriate intracellular destinations by active mechanisms involving molecular motors [1, 2]. Molecule sorting takes place on the plasma membrane, on inner membrane bodies (endosomes) and in the Golgi network. Common biochemical principles underlie molecule sorting in these different locations [3].

But what are the physical bases of sorting? Self-aggregation processes driven by reinforcing feedback loops lead to the formation of submicrometric domains enriched in specific lipids and proteins, and are ubiquitous on cell membranes [see 4, and references therein]. Moreover, the formation of molecular aggregates has been observed to precede and induce vesicle nucleation [5, 6], and evidences suggest that, by themselves, lipid accumulation [7, 8] and protein crowding [9, 10] can initiate membrane bending and vesicle nucleation by making these processes energetically favorable [11–14].

These observations suggest that sorting may be a universal process emerging from the coupling of two main

components: a) self-aggregation of localized lipid-protein microdomains, and b) vesicle nucleation. In this scheme, molecules that diffuse on a membrane can aggregate into localized enriched domains that grow due to molecule absorption. When a domain reaches a sufficiently large size, its biochemical constituents locally induce higher membrane curvature and the consequent nucleation and detachment of a small vesicle. The newly generated vesicle is constitutively enriched in the biochemical factors of the engulfed domain, resulting in a spontaneous distillation process.

Here, we investigate the consequences of this general scenario by comparing quantitative measures of the kinetics of endocytic sorting in living cells with a phenomenological theory expressed in terms of measurable quantities, and with numerical simulations of a lattice-gas model. In this framework, the average time spent by sorted molecules on the membrane is a natural measure of the efficiency of the sorting process. We find, somehow paradoxically, that higher efficiency is expected when molecules are sorted in the smallest possible number of sorting domains, a situation taking place for levels of self-aggregation that are neither too large nor too low. Our quantitative measures suggest that these optimal conditions are realized in living cells.

* kolokol@itp.ac.ru

† lebede@itp.ac.ru

‡ luca.dallasta@polito.it

§ andrea.gamba@polito.it

II. EXPERIMENTAL ANALYSIS OF ENDOCYTIC SORTING

We measured the kinetics of endocytic sorting on the plasma membrane of primary human endothelial cells (see App. C–F for details). Cells were maintained in a stationary state under constant nutrients uptake, while clathrin molecules, one of the main components of nascent lipid vesicles, were tagged with a fluorescent protein. The local density of fluorescently-tagged molecules was quantified using Total Internal Reflection Fluorescence (TIRF) microscopy (Fig. 1(a)), which allows to constrain the analysis to a thin layer of approximately 100 nm from the plasma membrane. In these experimental conditions it was possible to observe a large number of physiological endocytic events. An example of such an event, including the process of vesicle formation and detachment, is displayed in Fig. 1(c) (consecutive frames, with 10 s delay, are reported): the progressive appearance and sudden disappearance of a fluorescent circular domain in the middle of the selected region (red circle) corresponds to the growth and detachment of a clathrin-coated vesicle.

For each cell approximately one hundred vesicle formation events were identified. The typical time-dependent behavior of the fluorescence intensity of single events is reported in Fig. 1(b). Growing, fluorescently-tagged domains were identified by automated image analysis (see App. E, F for details). The fluorescence intensity of each domain was recorded at subsequent times. The total fluorescence intensity of a domain is proportional to its area. In order to fix the conversion factor between these two quantities, we assumed that the typical fluorescence intensity value reached by growing domains just before their extraction corresponds to the radius of mature clathrin-coated vesicles, $R_E \sim 50$ nm [15]. This way, histograms of domain radii were obtained (Fig. 1(d), thin color lines). The approximately linear dependence of the frequency density on domain size for radii $R < R_E$ suggests that the absorption of molecules that are freely diffusing on the plasma membrane could be the dominant mechanism for domain growth [16, 17].

III. PHENOMENOLOGICAL THEORY

To gain theoretical insight into the physical mechanism behind the observed experimental behavior we introduce here a phenomenological theory of molecular sorting. Such a theory allows in particular to study the efficiency of the process. A natural measure of sorting efficiency is the sorting rate, defined as the inverse of the average time \bar{T} spent by a molecule on the lipid membrane before extraction. A larger sorting rate corresponds to reduced protein recycling time and faster response to stimuli.

From the empirical data it is reasonable to assume that, under basal physiological conditions, molecule transport through the endocytic recycling pathway is in

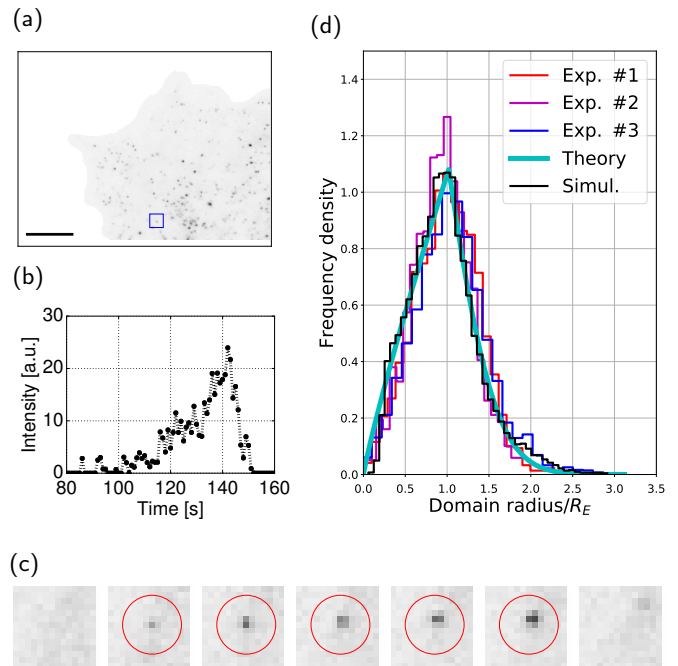


Figure 1. Sorting domains on the cell plasmamembrane. (a) TIRF micrograph of sorting domains; scale bar: 10 μ m; blue square: sample region of interest. (b) Time course of fluorescence intensity in the region of interest. (c) Snapshots of the region of interest separated by 10 s intervals, starting from 90 s (1 pixel: 180 nm); red circles are centered around an automatically identified growing domain. (d) Frequency density of domain radii: comparison of experiments (data for three distinct cells are shown) with phenomenological theory and numerical simulations of a lattice-gas model.

a regime in which molecules arrive on the membrane, diffuse and aggregate into localized enriched domains, and these domains are removed from the membrane, after reaching the characteristic size R_E , through the formation of small separate lipid vesicles. We therefore describe a situation in which sorting domains coexist in a statistically stationary state with a continuously replenished dilute solution, or “gas”, of molecules that diffuse freely on a membrane.

This is reminiscent of two-dimensional diffusion-limited aggregation, (DLA) [18] or Hele-Shaw problem [19]. It is well known that at the advanced stages, DLA leads to the formation of clusters with multifractal structure [18]. We assume, however, that in our case, due to the presence of the cutoff length R_E , which restricts the domain size, domain shapes do not strongly deviate from round ones, contrary to what takes place in the advanced stages of DLA.

As in the classical framework of Lifshitz-Slezov (LS) theory [16, 20], domains of size R larger than a critical value R_c grow irreversibly by means of the absorption of single molecules diffusing towards them. This mechanism is expected to provide the dominant contribution to the absorption dynamics for sufficiently small average

molecule density \bar{n} in the gas. For domains with sizes much larger than the critical size R_c , the density n_0 near the domain boundary is independent of its size. When the typical inter-domain distance L is much larger than R_E , the difference Δn in molecule density between the regions farther away and closer to the domain boundaries is approximately given by $\bar{n} - n_0 > 0$. Contrary to LS theory, in which domains can grow arbitrarily in time and Δn tends to zero as time grows, here the size of domains removed from the system introduces a cut-off length $R_E \gg R_c$, and, in the statistically stationary regime, Δn is kept finite by the continuous influx of particles into the system.

The density n of freely diffusing molecules in the vicinity of a domain can be evaluated, in the quasi-static approximation, solving the Laplace equation with Dirichlet boundary conditions. The quasi-static profile of density around a circular domain of size R is

$$n(r) = n_0 + \frac{\ln r/R}{\ln L/R} \Delta n, \quad (1)$$

where r is the distance from the domain center. Deviations of the domain shape from circularity produce rapidly decaying higher multipole contributions that may be neglected in the main approximation.

The domain grows due to the flux Φ_R of molecules from the gas, which can be found by integrating the flux density $-D \nabla n$ over a circle of radius $r \gg R$:

$$\Phi_R = 2\pi r D \partial_r n(r) = \frac{2\pi D \Delta n}{\ln(L/R)}, \quad (2)$$

where D is the diffusion coefficient of isolated molecules. From (2) one obtains the dynamic equation for domain growth,

$$\frac{dR}{dt} = \frac{A_0 D \Delta n}{R \ln(L/R)}, \quad (3)$$

where A_0 is the area occupied by a molecule in the domain, and the domain size R is defined in such a way that the domain area is πR^2 .

Abstracting from complicated molecular details, the mesoscopic effects of vesicle extraction will be encoded in a single parameter, the rate $\gamma(R)$ by which domains of size R are removed from the system. If $N(t, R) dR$ is the number of domains per unit area with size between R and $R + dR$, the number density $N(t, R)$ satisfies the Smoluchowski equation

$$\frac{\partial N}{\partial t} + \frac{\partial}{\partial R} \left[\frac{A_0 D N \Delta n}{R \ln(L/R)} \right] = -\gamma(R) N, \quad (4)$$

where (3) was used. A stationary solution of (4) is

$$N_{\text{st}}(R) = \frac{J R \ln(L/R)}{D \Delta n} \exp \left[- \int_0^R dr \frac{r \ln(L/r) \gamma(r)}{A_0 D \Delta n} \right], \quad (5)$$

where the factor J has to be determined in terms of the incoming flux ϕ .

Based on the experimental observations, we assume that the extraction rate $\gamma(R)$ is negligible for $R < R_E$ and strongly suppresses $N_{\text{st}}(R)$ for $R > R_E$, where R_E is the characteristic size of the domains that are extracted from the membrane. Our phenomenological approach is applicable if the inequality $R_E^2 \gg A_0$ is satisfied. This inequality also justifies the quasi-static approach leading to Eq. (1). In the region $R < R_E$ where $\gamma(R)$ is negligible, Eq. (5) shows that the distribution $N_{\text{st}}(R)$ has a universal behavior characterized by a linear growth (with logarithmic corrections). This agrees with the experimentally measured distribution of domain sizes (Fig. 1(d), thin color lines).

To fit the experimental data in the decaying part of the domain size distribution we model $\gamma(R)$ by a step (Heaviside's) function, equal to zero for $R < R_E$ and to a finite value γ_0 for $R > R_E$. By fitting the rate γ_0 , our phenomenological theory reproduces the experimental data also for sizes larger than R_E (Fig. 1(d), thick cyan curve). The constant J in Eq. (5) is determined by noticing that, in the stationary regime, the average flux $\int \Phi_R N_{\text{st}}(R) dR$ must equate the incoming flux of molecules per unit area ϕ , giving $J \sim \phi / R_E^2$.

The average time \bar{T} spent by a molecule in the system is the sum of the average time \bar{T}_f required by a molecule to reach a domain by free diffusion and be absorbed, and the average time \bar{T}_d spent by the molecule inside that domain until the extraction event. For evenly distributed domains, the first contribution \bar{T}_f is inversely proportional to the average number N_d of domains per unit area, where

$$N_d = \int dR N_{\text{st}}(R) \sim \frac{\phi}{D \Delta n}, \quad (6)$$

giving

$$\bar{T}_f \sim \frac{1}{D N_d} \sim \frac{\Delta n}{\phi}. \quad (7)$$

In its turn, the average time spent by a molecule in a domain can be estimated as

$$\bar{T}_d \sim \frac{R_E^2}{A_0 \Phi_R} \sim \frac{R_E^2}{D A_0 \Delta n}, \quad (8)$$

where (2) was used.

The rate of formation of new domains can be estimated as

$$\frac{dN_d}{dt} = C D \bar{n}^2, \quad (9)$$

where C is a dimensionless quantity characterizing the efficiency of absorption of single molecules by the germ of a domain. In the stationary condition the rate (9) is equal to N_d / \bar{T}_d , therefore

$$\bar{n} \sim \left(\frac{\phi A_0}{C D R_E^2} \right)^{1/2}. \quad (10)$$

Assuming $n_0 \lesssim \Delta n$ we get $\Delta n \sim \bar{n}$ and then

$$\bar{T}_d \sim C^{1/2} \frac{R_E^3}{(D\phi)^{1/2} A_0^{3/2}}, \quad \bar{T}_f \sim C^{-1/2} \frac{A_0^{1/2}}{(D\phi)^{1/2} R_E}. \quad (11)$$

The sum $\bar{T} = \bar{T}_d + \bar{T}_f$, as a function of C , has a minimum in $C \sim A_0^2/R_E^4 \ll 1$, where

$$\bar{T}_f \sim \bar{T}_d \sim \frac{R_E}{(DA_0)^{1/2} \phi^{1/2}}, \quad (12)$$

$$\bar{n} \sim \Delta n \sim \frac{\phi^{1/2} R_E}{(DA_0)^{1/2}}. \quad (13)$$

Therefore, the scaling relations (12,13) identify the dynamical regime in which molecular sorting is most efficient. The density of molecules accumulated in the domains is

$$\rho_d \sim N_d R_E^2 / A_0 \sim C^{1/2} \frac{\phi^{1/2} R_E^3}{D^{1/2} A_0^{3/2}}. \quad (14)$$

Thus, also the total density $\rho = \bar{n} + \rho_d$ has a minimum for $C \sim A_0^2/R_E^4$, and the minimal value of ρ is again determined by the estimate (13).

IV. LATTICE-GAS MODEL AND NUMERICAL RESULTS

Stochastic lattice-gas models provide a natural framework to study the non-equilibrium steady-states of driven particle systems [21, 22] and have been applied to elucidate several aspects of intracellular transport [23–26]. To further explore the role of molecule self-aggregation in the distillation process, and to probe the behavior of the sorting process over a wide range of parameter values, we introduce here a minimal lattice-gas model of molecular sorting.

We represent the lipid membrane as a two-dimensional square lattice with periodic boundary conditions. Each lattice site can host a single molecule, so that the current state of the system is completely described by a multivariate binary configuration providing the number, 0 or 1, of molecules at every site. This binary configuration is assumed to evolve according to a Markov process that comprises the following three elementary mechanisms: 1) Molecules from an infinite reservoir arrive and are inserted on empty sites with rate k_I . 2) Then, molecules can perform diffusive jumps to an empty neighboring site

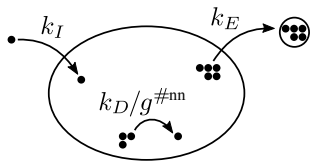


Figure 2. Minimal model for molecular sorting.

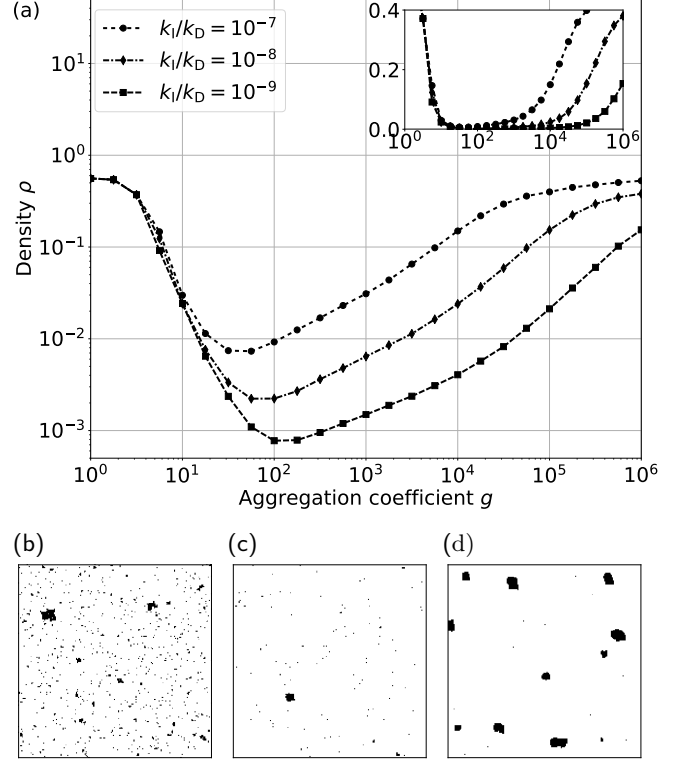


Figure 3. (a) Molecule density ρ (time average in the stationary state) as a function of the aggregation coefficient g , for $k_I/k_D = 10^{-7}, 10^{-8}, 10^{-9}$. Inset: same quantities in log-linear scale. (b)–(d) Snapshots of configurations obtained with $k_I/k_D = 10^{-7}$ and $g = 10, 30, 300$ (from left to right; pictures show one quarter of a simulated system of 400^2 sites).

with rate $k_D/g^{\#nn}$, where $g > 1$ is a dimensionless aggregation coefficient and $\#nn$ is the number of neighboring molecules in the original position of the jumping molecule. 3) Finally, molecules are extracted from the system by the simultaneous removal at rate k_E of all connected molecule clusters, if any, that contain a completely filled square of linear size ℓ , with $\ell^2 \sim R_E^2/A_0$. This last process represents in a stylized way the extraction of sorting domains of size larger than R_E by means of the localized nucleation and detachment of small lipid vesicles, without any attempt at a complete description of the complex biochemical and physical details implied in the process of vesicle budding and removal. A schematic description of the model is shown in Fig. 2. Its formal mathematical definition is given in App. A.

The model was investigated by performing numerical simulations in the limit $k_E \rightarrow \infty$. This way, the stationary properties of the model depend on only two parameters, the ratio k_I/k_D and the aggregation coefficient g . It is worth observing here that the precise value of the extraction rate is irrelevant as long as the extraction dynamics is much faster than the characteristic timescale of

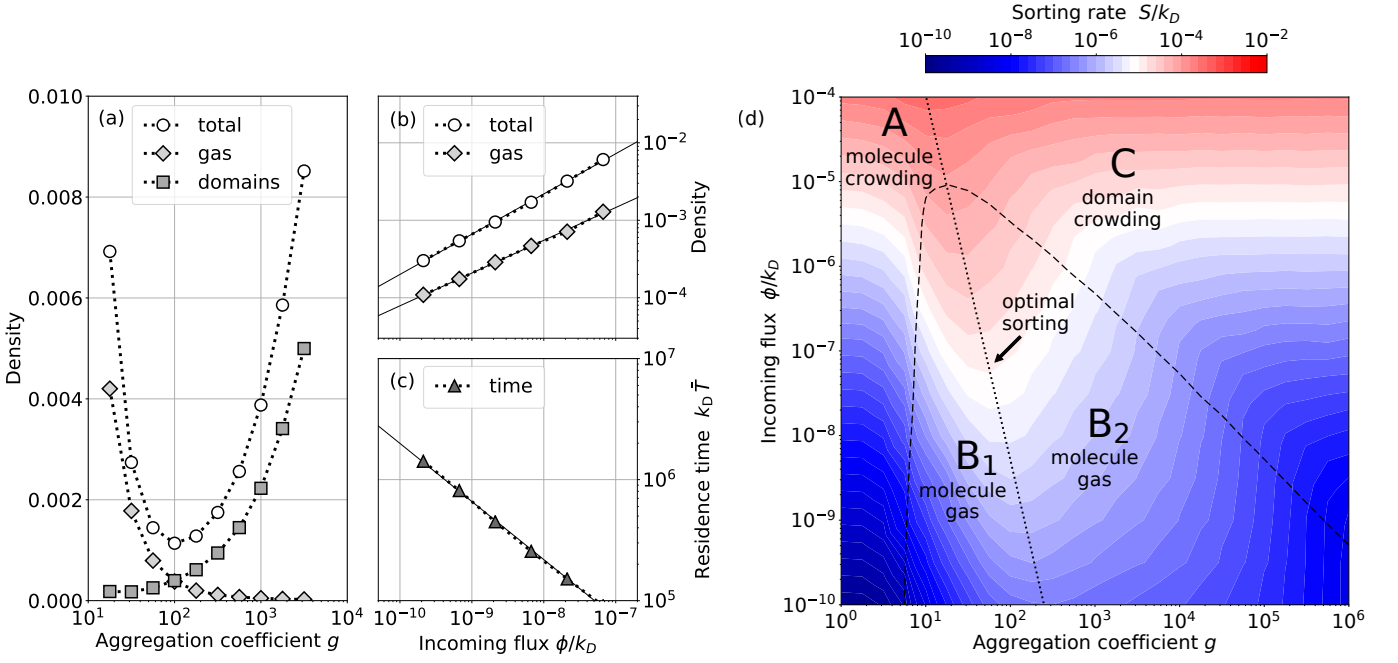


Figure 4. (a) Partial molecule densities as functions of the aggregation coefficient g . The density of the gas component decreases, while the number of molecules in the interior of sorting domains increases for increasing g at fixed $\phi/k_D = 10^{-8}$ and infinite k_E ; as a consequence, the total molecule density has a minimum at an intermediate value of g . (b-c) Numerical evidence of scaling relations for infinite k_E . Straight lines are fitted with the laws $\rho \sim \phi^a$, $\bar{n} \sim \phi^b$, and $\bar{T} \sim \phi^{-c}$ with $a = 0.52 \pm 0.01$, $b = 0.46 \pm 0.01$, and $c = 0.48 \pm 0.01$. (d) Sorting rate S as a function of the aggregation coefficient g and of the incoming flux ϕ , with infinite k_E . At fixed ϕ , faster distillation takes place for intermediate values of g , thus showing the existence of a region of parameter space where sorting is optimal. In this qualitative phase diagram, A, C are high-density phases, characterized by molecule crowding and domain crowding, respectively; B is a low-density phase. The dotted line marks maximal sorting at fixed flux ϕ , and divides the B region into regions of less (B₁) and more dilute gas (B₂).

domain growth, so that similar scenarios are always observed for large but finite values of k_E . In what follows, areas are measured in units of a lattice site, therefore $A_0 = 1$, and the particle densities ρ , n are dimensionless quantities.

Fig. 3(a) shows the stationary density of molecules ρ , i.e. the mean fraction of occupied sites, as a function of the aggregation coefficient g , for several values of k_I/k_D . Low values of the aggregation coefficient g make aggregation unlikely, consequently large compact domains are rare and the extraction of vesicles is infrequent, thus resulting in high values of ρ . For such values of g the system is dominated by a dense gas of diffusing molecules. For large values of g , several sorting domains compete with each other to reach the extraction size; the pool of free molecules that can feed these growing domains is now scarce, consequently the extraction size is rarely achieved and the density of molecules is again large. The density is instead low for intermediate values of g , where a dilute gas of free molecules coexists with growing sorting domains, such as those shown in Fig. 3(b)–(d). In this region, the fraction of free molecules decreases as g is increased, while the total molecule density reaches a minimum in Fig. 3(c). The neighborhood of this minimum corresponds to the region previously found from the

analysis of the phenomenological theory, which is likely to be the most interesting from the biological point of view. The assumptions that domains are well separated and that their shapes do not deviate strongly from round ones are consistent with the results of numerical simulations (Fig. 3(b)–(d)).

In Fig. 4(a) the total density ρ is decomposed into the contributions of freely diffusing molecules and of the molecules which are part of sorting domains. When g is increased, the density of freely diffusing molecules decreases, whereas the number of molecules in the domains increases, explaining the appearance of a minimum of ρ (Fig. 4(a), white circles) at intermediate values of the aggregation coefficient g . In this region, we compute numerical scaling relations with respect to the incoming flux per unit site $\phi = k_I(1 - \rho)$, finding good agreement with the theoretical predictions (12) (Fig. 4(b)–(c) and figure legend); the small discrepancy in the second digit of the scaling exponents is not unexpected, considering that logarithmic corrections were neglected in the equations.

To characterize the efficiency of the sorting process we computed numerically the sorting rate $S = \bar{T}^{-1} = \phi/\rho$ (see App. B and Ref. [27]) in terms of the physically meaningful parameters ϕ and g [28]. Fig. 4(d) shows that S increases monotonically with ϕ , and that it exhibits a

maximum as a function of g at fixed ϕ (the dotted line in Fig. 4(d) marks the position of these maxima). Distillation of molecular factors is most efficient in the optimal sorting region located around the maxima of S . The dashed line in Fig. 4(d) separates regions A and C with high molecule density from regions B₁ and B₂, characterized by lower densities. The two “phase boundaries”, merging for large values of the incoming flux, have clearly different properties at lower ϕ . The A–B₁ boundary is the inheritance, in the non-equilibrium driven system, that characterizes the phase separation of unbalanced binary mixtures. The boundary between regions B₂ and C marks instead the occurrence of a percolation-like transition that, preventing free diffusion of isolated molecules, inhibits the primary mechanism for domain growth and, consequently, their extraction.

These features emerging from the numerical simulations are in agreement with the phenomenological theory. This is easily seen by considering that, in the framework of the numerical scheme, the efficiency C of absorption of single molecules increases monotonically with g . Then the existence of the maximum of the sorting rate $S = \bar{T}^{-1}$ and of the minimum of the density ρ observed in the numerical modeling appears as a natural consequence of the phenomenological theory. Moreover, the contrasting behavior of the density of particles in the gas and in the domains (see Fig. 4(a)) agrees with Eqs. (10,14).

It is interesting to check how experimental data compare with our physical theory. In the experiments described in Sec. II we measured densities and fluxes $\rho^{\text{exp}} = (2.2 \pm 0.8) \cdot 10^{-3}$, $\phi^{\text{exp}} = (1.6 \pm 0.3) \cdot 10^{-5}$, expressed, respectively, as fraction of the cell surface covered by sorting domains, and fraction of the cell surface extracted per second (see App. F for details). The microscopic rate k_D can be roughly estimated as D/A_0 , where $D \sim 0.05\text{--}0.5 \mu\text{m}^2/\text{s}$ is the diffusivity of common plasma membrane bound proteins [29], and $A_0 \sim (10 \text{ nm})^2$ is the lateral surface occupied by a protein [30]. The relation $\phi^{\text{exp}} = k_I(1 - \rho^{\text{exp}}) \simeq k_I$ allows then to estimate $k_I/k_D \sim 10^{-8}\text{--}10^{-9}$. Fig. 3(a) shows that for such parameter values, experimentally measured densities are attained in the physical model in the vicinity of the minima of the density ρ , i.e in the optimal region, where $g \sim 10^2$. We used this parameter choice to estimate k_E from the experiments by fitting the decaying tail of the domain size distribution (Fig. 1(c), black line), finding $k_E \sim 10^3 k_I$. The phase diagram computed for such finite values of k_E (Fig. 5) does not differ significantly from the one with infinite k_E (Fig. 4(d)) [31]. On this phase diagram, compatible g, ϕ pairs are found from the intersections of numerically computed $\rho(g, \phi) = \rho^{\text{exp}}$, $\phi = \phi^{\text{exp}}$ isolines. By taking into account experimental uncertainties and the range of variation $0.05\text{--}0.5 \mu\text{m}^2/\text{s}$ for D , the extended compatibility region shown as a dashed area in Fig. 5, which lies in a neighborhood of the optimal sorting line, is finally obtained (qualitatively indistinguishable results are obtained for infinite k_E).

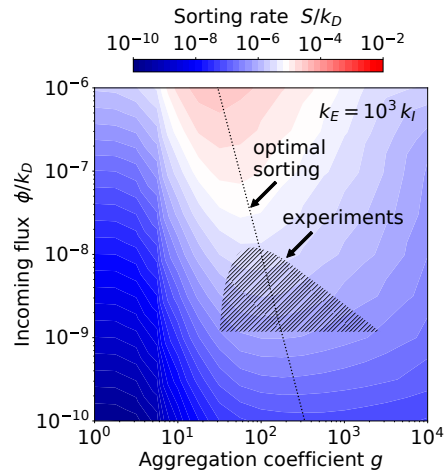


Figure 5. Identification of model parameters compatible with experimental values of density and flux. A finite extraction rate k_E , compatible with the experimental spread in the size of extracted domains (Fig. 1d), was used. The set of compatible parameter values, shown as a dashed area, lies in a neighborhood of the optimal sorting line.

V. DISCUSSION

Observing living eukaryotic cells under a fluorescence microscope in real time, one is immediately struck by the hectic and apparently chaotic traffic of a myriad of sub-micrometric vesicles that transport lipids and proteins to the most disparate subcellular locations [32]. This restless movement takes place at significant energy cost, suggesting that it must be deeply relevant for cell life. Actually, to perform its main vital tasks, such as feeding on nutrients, proliferating, migrating, and forming sophisticated multicellular tissues, the cell, which is basically a droplet of fluid enclosed in a thin lipid envelope, has first of all to break its symmetry [33, 34]. As a result of this symmetry breaking, each particular region of both surface and organelle membranes becomes endowed with a specific chemical identity, that allows it to perform its peculiar functions [34]. Vesicular traffic is one of the main processes that create and sustain this broken-symmetry state: vesicles enriched in specific molecular factors are delivered to appropriate membrane regions to maintain those regions’ biochemical identity and contrast the homogenizing effect of diffusion [35]. To sustain the process, a never ending source of enriched vesicles is required, implying that the needed molecular factors must be continuously distilled and packaged on such vesicles.

What are the physical bases of this universal distillation process? We have proposed here a scenario whereby distillation emerges naturally from the coupling of two spontaneous processes: a) molecular self-aggregation, and b) vesicle nucleation. This view has solid bases in the physical chemistry of vesicular traffic. Several mechanisms have been identified that link the formation of molecular aggregates to the induction of membrane

bending and vesicle nucleation [9–13]. It is also well known that the main proteins involved in the generation of enriched vesicles at different subcellular compartments share the following set of features: i) can bind to cell membranes, ii) tend to self-aggregate, iii) can bend membranes, iv) can bind the proteins to be distilled [36].

Abstracting from molecular details, the following picture emerges: a continuously repleted gas of molecules diffusing towards multiple sorting centers that grow due to molecular absorption and are extracted when reaching a sufficiently large size, leading to the formation of a vesicle in which a higher-than-average concentration of the given molecular factor has been distilled. From this abstract scenario, some general results follow. The sizes of sorting domains below the extraction threshold should be linearly distributed, up to logarithmic corrections. This theoretical prediction is corroborated by numerical simulations and is in agreement with experiments, confirming the validity of the general physical picture. The sorting process is most efficient when the tendency of molecules to aggregate in microdomains is neither too low nor too large, pointing out at the central role of self-aggregation in ordering the system. When the strength of aggregation is too low, the sorting process is inefficient. On the other hand, when the strength of aggregation is too high, sorting domains proliferate and compete with each other for the binding of free molecules, thus slowing down the sorting process.

The emergence of an optimal sorting regime at intermediate values of the aggregation strength is a nontrivial effect of the physics of diffusion-limited aggregation processes on cell membranes. In this optimal regime, both the density \bar{n} of freely diffusing molecules and the total molecule density ρ are minimal. By measuring the density of sorting domains and the sorting flux, we observed that primary cells kept in basal, steady-state physiological conditions live close to this optimal regime. It is tempting to speculate that an evolutionary constraint may have led the proteins responsible for the distillation process to tune their activity around optimality, due to the selective advantage provided by maximal sorting efficiency.

Here for simplicity we considered the distillation of a single molecular factor. It is however immediately evident that distinct clans of molecules endowed with high intra-clan affinity can aggregate independently and be sorted in parallel. Moreover, a spontaneous process of diffusion-limited chemical phase separation may lead molecules belonging to such clans to aggregate in “soft” enriched domains even without direct physical interaction, if they participate in a network of catalytic reinforcing feedback loops [4, 20, 37]. With the establishment of super-resolution microscope techniques, much evidence has been accumulated about the ubiquitous formation of transient, stochastic protein nanodomains on lipid membranes [38, 39]. The origin of this enigmatic spatio-temporal structure is still partially unclear. It is worth observing here that in the light of the present sce-

nario, it would be natural to expect precisely this kind of spatio-temporal organization as the result of the incessant, parallel distillation of a multitude of molecular factors on both surface and organelle membranes.

ACKNOWLEDGMENTS

MZ, LDA and AG thank Carlo Cosimo Campa, Jean Piero Margaria and Emilio Hirsch for useful discussions. Numerical calculations have been made possible through a CINECA-INFN agreement providing access to resources on MARCONI at CINECA.

Appendix A: Lattice-gas model

The computational model is defined on a periodic square lattice containing L^2 sites. The presence/absence of a molecule on site i is denoted by the binary variable η_i . The kinetics of distillation is described by the continuous-time Markov process specified by the infinitesimal generator $\mathcal{L} = \mathcal{L}_I + \mathcal{L}_D + \mathcal{L}_E$, whose components are the generators for molecule insertion, diffusion-aggregation, and extraction defined as follows. We recall here that if $f(\eta)$ is a function of the state $\eta = \{\eta_i\}$, the generator \mathcal{L} of the process is the operator defined by the relation $\partial_t f(\eta) = \mathcal{L}f(\eta)$.

Insertion – Molecules are inserted at empty sites with insertion rate k_I :

$$\mathcal{L}_I f(\eta) = k_I \sum_i (1 - \eta_i) [f(\eta^i) - f(\eta)]$$

where the configuration η^i differs from η only for the insertion of a molecule on site i .

Diffusion and aggregation – Molecules can jump on empty neighboring sites:

$$\mathcal{L}_D f(\eta) = k_D \sum_i \sum_{j \in N_i} \eta_i (1 - \eta_j) g_i(\eta) [f(\eta^{ij}) - f(\eta)]$$

where N_i are the nearest neighbors of i , the configuration η^{ij} differs from η only for the jump of a molecule from i to j , and the factor

$$g_i(\eta) = \prod_{k \in N_i} g^{-\eta_k}$$

reduces the probability of jumps that break links with neighboring occupied sites. High values of the aggregation coefficient $g \geq 1$ favor the formation of molecular aggregates.

Extraction – Connected components containing at least a square region V of linear size ℓ completely filled with molecules are extracted with rate k_E :

$$\mathcal{L}_E f(\eta) = k_E \sum_{C \in \mathcal{C}} h \left(\sum_{V \subset C} \prod_{j \in V} \eta_j \right) [f(\eta^C) - f(\eta)]$$

where \mathcal{C} is the collection of connected subsets of the lattice, $h(x) = 0$ for $x = 0$, $h(x) = 1$ for $x > 0$, V is a square region of linear size ℓ , and the configuration η^C is obtained from η by emptying all of the sites in C . Simulations were performed with $L = 400$ and $\ell = 10$ using Gillespie's algorithm [40].

Appendix B: Molecule flux and residence time

The average number of molecules inserted into the membrane system per site and per unit time is given by

$$\phi = k_I (1 - \rho)$$

since molecules can only be inserted at empty sites.

Areas are measured here in units of a lattice site. In the statistically stationary state, ϕ coincides with the flux of extracted molecules. Since there can be at most a single molecule per site, ϕ can also be interpreted as the fraction of membrane area extracted from the system per unit time. Numerical simulations of the statistically stationary state show that ϕ is a monotonically increasing function of k_I at fixed g (Fig. 6).

Let the time T spent by a molecule on the membrane system in the statistically stationary state be a stochastic variable with probability density $p(t)$. The average number ρ of particles per site that are found on the membrane system at time $t = 0$ is the sum of the ϕdt particles introduced in average during the previous time intervals of duration dt , such that their permanence time has not yet elapsed:

$$\begin{aligned} \rho &= \int_0^\infty \text{Prob}(T > t) \phi dt = \phi \int_0^\infty \left(\int_t^\infty p(\tau) d\tau \right) dt \\ &= \phi \int_0^\infty t p(t) dt = \phi \bar{T} \end{aligned}$$

The average residence time of a molecule in the system is therefore $\bar{T} = \rho/\phi$. This exact relation holds for a large class of stochastic lattice-gas models with general injection, diffusion and extraction dynamics [27].

Appendix C: Cell culture

Primary arterial endothelial cells (AECs) were isolated from the umbilical cords as previously described [41] and grown in Endothelial Cell Growth Basal Medium (EBM-2) supplemented with EGM-2 BulletKit (Lonza Basel, Switzerland) (EGM-2). The isolation of primary arterial ECs human umbilical cords was approved by the Office of the General Director and Ethics Committee of the Azienda Sanitaria Ospedaliera Ordine Mauriziano di Torino hospital (protocol approval no. 586, Oct 22 2012 and no. 26884, Aug 28 2014) and informed consent was obtained from each patient. Fluorescent tagged EYFP-Clathrin was a gift from Xiaowei Zhuang, Harvard University, Cambridge, MA (Addgene plasmid #20921) [42].

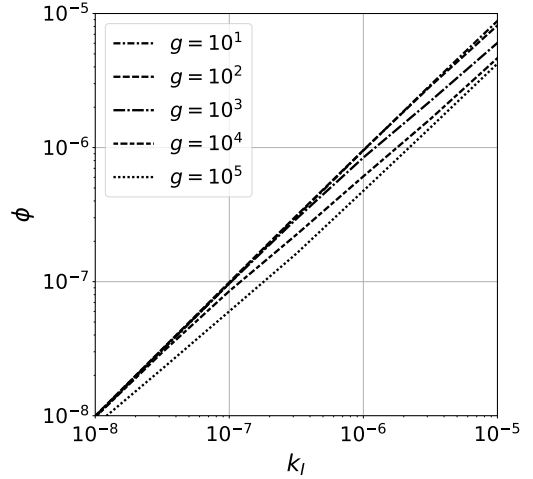


Figure 6. In the statistically stationary state, ϕ is a monotonically increasing function of k_I at fixed g .

Plasmid DNA was electroporated in AECs with Ingenio Electroporation Kit (Mirus Bio LLC, Madison, USA).

Appendix D: Time-lapse TIRF microscopy

TIRF microscopy on living ECs was performed using a Leica AM TIRF MC system mounted on a Leica AF 6000LX workstation. Cells were plated onto glass-bottom dishes (WillCo-dish; Willcowells, Amsterdam, The Netherlands) coated with $3 \mu\text{g/ml}$ human plasma fibronectin (1918-FN-02M, R&D, Systems, Minneapolis, MN, USA) and placed onto a sample stage within an incubator chamber set to 37°C , in an atmosphere of 5% CO_2 , 20% humidity. A Leica HC PL APO $63\times/1.47$ NA oil-immersion objective was used, and laser penetration depth was set at 90 nm. Excitation and analysis of fluorescent proteins were performed with a 488 nm laser. Imaging was recorded on a Hamamatsu EM-CCD camera (C9100-02, Hamamatsu, SZK, Japan).

Appendix E: Image processing

Photograms from time-lapse TIRF microscopy (1s time intervals, 180 nm pixel resolution) were analyzed. Fluorescent domains were automatically recognized. Domains were tracked based on the overlap of their images between subsequent photograms. Only domains appearing after the first frame and disappearing earlier than the last frame were considered. For each domain, the net cumulative fluorescence intensity was collected from a circular region centered on the domain after subtracting the average background signal. The correspondence between areas and fluorescence intensi-

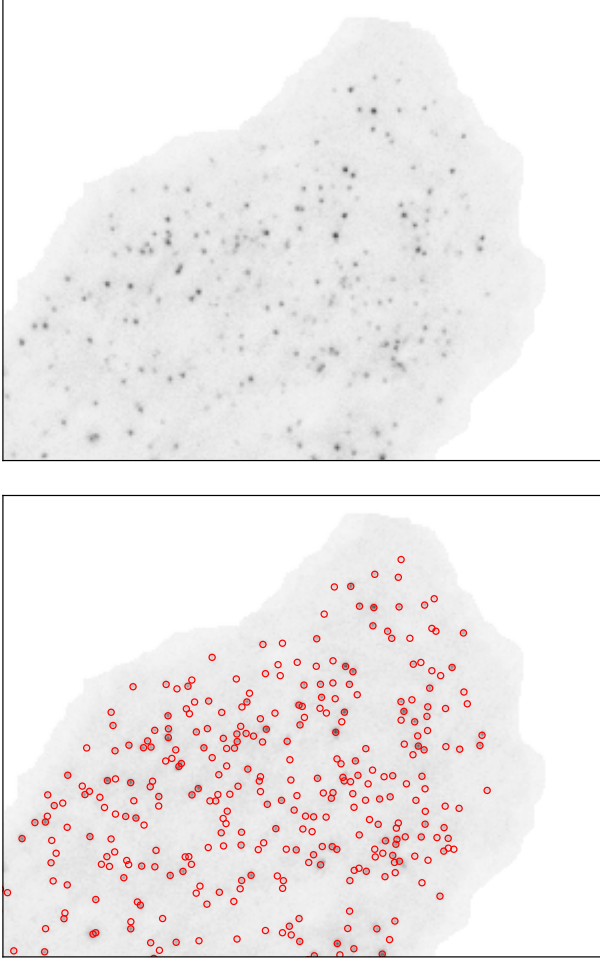


Figure 7. Automatic recognition of endocytic domains. Top: TIRF image of fluorescent domains. Bottom: red circles identify automatically recognized domains.

ties was established by associating the average surface of a clathrin-coated vesicle to the maximum of the statistical distribution of fluorescence intensities. From these data, estimates of the average domain density and the average rate of endocytic events were computed (see App. F).

Appendix F: Measure of density and flux

Photograms from movies of 200 s duration separated by 1 s time intervals were analyzed using the open-source software SciPy (scipy.org) and OpenCV (opencv.org). A binary mask was used to isolate single cells from images containing more than one cell. Fluorescent circular domains were identified using the blob detection algorithm implemented by the OpenCV command SimpleBlobDetector. Visual inspection suggests that the number of wrongly identified domains did not exceed 1% (Fig. 7).

Background fluorescence intensity was computed as the average of the fluorescence intensity of pixels outside of circular domains. Domains whose images overlapped in two subsequent photograms were identified and their centers computed. Net fluorescence intensity values $I_{f,p}$ were collected from each frame f and pixel p after background subtraction. For each domain d , the cumulative fluorescence intensity was computed as $I_{d,f} = \sum_{p \in C_{f,d}} I_{f,p}$, with $C_{f,d}$ the circle of radius 500 nm centered on domain d . To restrict the analysis to real endocytic events, domains were ranked according to descending values of cumulative square deviations from the time average and histograms of fluorescence intensity were computed from the first percentile. The peak value I_E was derived from the histograms, and the maximum value $I_d = \max_f (I_{d,f})$ was computed for each domain d . The same procedure was applied to the analysis of the size of simulated domains, except that in that case $I_{d,f}$ was the number of occupied sites in a domain.

Experimental estimates of the fraction ρ of membrane area covered by sorting domains, and the fraction ϕ of membrane area extracted per photogram (and therefore per second) were computed as

$$\rho = \frac{1}{M} \sum_f \sum_d \frac{I_{d,f}}{I_E} \frac{A_E}{A}$$

$$\phi = \frac{1}{M} \sum_{I_d > I_E} \frac{I_d}{I_E} \frac{A_E}{A}$$

where $A_E = 4\pi R_E^2$ is the area of membrane extracted during an endocytic event, A is the area of the cell membrane observed in the experiment, and M is the number of photograms. The dimensionless density ρ and the dimensionless ratio ϕ/k_D were used in the comparison with numerical simulations.

-
- [1] I. Mellman and W. J. Nelson, Nat. Rev. Mol. Cell Biol. **9**, 833 (2008).
 - [2] S. Sigismund, S. Confalonieri, A. Ciliberto, S. Polo, G. Scita, and P. P. D. Fiore, Physiol Rev **92**, 273 (2012).
 - [3] L. M. Traub, Biochim Biophys Acta **1744**, 415 (2005).
 - [4] M. Zamparo, F. Chianale, C. Tebaldi, M. Cosentino-Lagomarsino, M. Nicodemi, and A. Gamba, Soft Matter **11**, 838 (2015).
 - [5] A. P. Liu, F. Aguet, G. Danuser, and S. L. Schmid, J Cell Biol **191**, 1381 (2010).
 - [6] C. Puri, D. Tosoni, R. Comai, A. Rabellino, D. Segat, F. Caneva, P. Luzzi, P. P. D. Fiore, and C. Tacchetti, Molecular Biology of the Cell **16**, 2704 (2005).
 - [7] L. Johannes and S. Mayor, Cell **142**, 507 (2010).
 - [8] T. S. Ursell, W. S. Klug, and R. Phillips, Proceedings of the National Academy of Sciences **106**, 13301 (2009).

- [9] D. J. Busch, J. R. Houser, C. C. Hayden, M. B. Sherman, E. M. Lafer, and J. C. Stachowiak, *Nat Commun* **6**, 7875 (2015).
- [10] J. C. Stachowiak, E. M. Schmid, C. J. Ryan, H. S. Ann, D. Y. Sasaki, M. B. Sherman, P. L. Geissler, D. A. Fletcher, and C. C. Hayden, *Nature cell biology* **14**, 944 (2012).
- [11] S. Leibler, *Journal de Physique* **47**, 507 (1986).
- [12] S. Leibler and D. Andelman, *Journal de physique* **48**, 2013 (1987).
- [13] A. Banerjee, A. Berezhevskii, and R. Nossal, *Biophys J* **102**, 2725 (2012).
- [14] L. Foret and P. Sens, *Proceedings of the National Academy of Sciences* **105**, 14763 (2008).
- [15] T. Kirchhausen, D. Owen, and S. C. Harrison, *Cold Spring Harbor perspectives in biology* **6**, a016725 (2014).
- [16] V. V. Slezov, *Kinetics of First Order Phase Transitions* (Wiley-VCH Verlag GmbH & Co. KGaA, Weinheim, 2009).
- [17] P. L. Krapivsky, S. Redner, and E. Ben-Naim, *A Kinetic View of Statistical Physics* (Cambridge University Press, 2010).
- [18] A.-L. Barabasi and H. E. Stanley, *Fractal Concepts in Surface Growth* (Cambridge University Press, Cambridge, 1995).
- [19] H. S. Hele-Shaw, *Nature* **58**, 34 (1898).
- [20] A. Gamba, I. Kolokolov, V. Lebedev, and G. Ortenzi, *Phys Rev Lett* **99**, 158101 (2007).
- [21] L. Bertini, A. D. Sole, D. Gabrielli, G. Jona-Lasinio, and C. Landim, *Journal of Statistical Mechanics: Theory and Experiment* **2007**, P07014 (2007).
- [22] J. Marro and R. Dickman, *Nonequilibrium Phase Transitions in Lattice Models (Collection Alea-Saclay: Monographs and Texts in Statistical Physics)* (Cambridge University Press, 2005).
- [23] P. C. Bressloff and J. M. Newby, *Rev Mod Phys* **85**, 135 (2013).
- [24] S. Klumpp and R. Lipowsky, *Phys Rev Lett* **95**, 268102 (2005).
- [25] I. Neri, N. Kern, and A. Parmeggiani, *Phys Rev Lett* **110**, 098102 (2013).
- [26] E. Reithmann, L. Reese, and E. Frey, *Phys Rev Lett* **117**, 078102 (2016).
- [27] M. Zamparo, L. Dall'Asta, and A. Gamba, *Journal of Statistical Physics* (2018), 10.1007/s10955-018-2175-x.
- [28] Since ϕ is a monotonically increasing function of the insertion rate k_I (see App. B), by a change of variable ϕ (which is directly observable) can be used as a control parameter in the place of k_I (which is not observable).
- [29] F. Daumas, N. Destainville, C. Millot, A. Lopez, D. Dean, and L. Salomé, *Biophysical journal* **84**, 356 (2003).
- [30] B. Alberts, A. Johnson, J. Lewis, M. Raff, K. Roberts, and P. Walter, *Molecular Biology of the Cell*, 4th ed. (Garland Science, New York, 2006).
- [31] This is not surprising, as the value of k_E obtained from the fit corresponds to a spread of order 2 in the size of extracted domains (Fig. 1c) and is therefore not expected to significantly modify the qualitative picture emerging from the infinite k_E case (Fig. 4d). It is also worth observing here that the properties of the decaying tail are not expected to be universal, as they are linked to details of the mechanism of vesicle removal, which involve a complicated molecular machinery responsible for inducing bending and removal of the vesicle [36].
- [32] B. Sönnichsen, S. De Renzis, E. Nielsen, J. Rietdorf, and M. Zerial, *J Cell Biol* **149**, 901 (2000).
- [33] R. Wedlich-Soldner and R. Li, *Nat Cell Biol*, 267 (2003).
- [34] E. Rodriguez-Boulán and I. G. Macara, *Nature reviews Molecular cell biology* **15**, 225 (2014).
- [35] A. Shewan, D. J. Eastburn, and K. Mostov, *Cold Spring Harb Perspect Biol*, a004796 (2011).
- [36] H. Shen, M. Pirruccello, and P. De Camilli, *Cell* **150**, 1300 (2012).
- [37] A. Gamba, A. de Candia, S. Di Talia, A. Coniglio, F. Bussolino, and G. Serini, *Proceedings of the National Academy of Sciences* **102**, 16927 (2005).
- [38] F. Spira, N. S. Mueller, G. Beck, P. von Olshausen, J. Beig, and R. Wedlich-Söldner, *Nat Cell Biol* **14**, 640 (2012).
- [39] M. F. Garcia-Parajo, A. Cambi, J. A. Torreno-Pina, N. Thompson, and K. Jacobson, *J Cell Sci* **127**, 4995 (2014).
- [40] D. T. Gillespie, *Journal of Computational Physics* **22**, 403 (1976).
- [41] G. Mana, F. Clapero, E. Panieri, V. Panero, R. T. Böttcher, H.-Y. Tseng, F. Saltarin, E. Astanina, K. I. Wolanska, M. R. Morgan, M. Humphries, M. Santoro, G. Serini, and D. Valdembrì, *Nature communications* **7**, 13546 (2016).
- [42] M. J. Rust, M. Lakadamyali, F. Zhang, and X. Zhuang, *Nature Structural and Molecular Biology* **11**, 567 (2004).